

#859

HEAD 1
X-Ray Source Catalog

77-075A-01C ASXR-00066



Table of Contents

1. Introduction
2. Errata/Change Log
3. LINKS TO RELEVANT INFORMATION IN THE ONLINE NSSDC INFORMATION SYSTEM
4. Catalog Materials
 - a. Associated Documents
 - b. Core Catalog Materials

1. INTRODUCTION:

The documentation for this data set was originally on paper, kept in NSSDC's Data Set Catalogs (DSCs). The paper documentation in the Data Set Catalogs have been made into digital images, and then collected into a single PDF file for each Data Set Catalog. The inventory information in these DSCs is current as of July 1, 2004. This inventory information is now no longer maintained in the DSCs, but is now managed in the inventory part of the NSSDC information system. The information existing in the DSCs is now not needed for locating the data files, but we did not remove that inventory information.

The offline tape datasets have now been migrated from the original magnetic tape to Archival Information Packages (AIP's).

A prior restoration may have been done on data sets, if a requestor of this data set has questions; they should send an inquiry to the request office to see if additional information exists.

2. ERRATA/CHANGE LOG:

NOTE: Changes are made in a text box, and will show up that way when displayed on screen with a PDF reader.

When printing, special settings may be required to make the text box appear on the printed output.

Version	Date	Person	Page	Description of Change
01				
02				

3 LINKS TO RELEVANT INFORMATION IN THE ONLINE NSSDC INFORMATION SYSTEM:

<http://nssdc.gsfc.nasa.gov/nmc/>

[NOTE: This link will take you to the main page of the NSSDC Master Catalog. There you will be able to perform searches to find additional information]

4. CATALOG MATERIALS:

- a. Associated Documents To find associated documents you will need to know the document ID number and then click here.
<http://nssdcftp.gsfc.nasa.gov/miscellaneous/documents/>

- b. Core Catalog Materials

HEAO 1

X-RAY SOURCE CATALOG

ASXR-00066

77-075A-01C

THIS DATA SET WAS NEVER ARCHIVED TO TAPE. IN 2005 AN ASCII VERSION

WAS DOWNLOADED FROM THE ASTRONOMICAL DATA CENTER (ADC) ARCHIVES.

THIS DATA SET HAS BEEN PROCESSED TO ONE CD-WRITE ONCE CONTAINING TWO FILES:

FILE 1 CONTAINS THE X-RAY SOURCE CATALOG AND FILE 2 CONTAINS THE DATA SET

DOCUMENTATION.

KD#	KW#	VOLUME	
-----	-----	-----	
KD023048	KW000209	HEAO-1_X-RAY	FILE 1 SOURCE.DAT FILE 2 README

The HEAO A-1 X-Ray Source Catalog

Wood K.S., Meekins J.F., Yentis D.J., Smathers H.W., McNutt D.P.,
 Bleach R.D., Byram E.T., Chubb T.A., Friedman H., Meidav M.
 <Astroph. Jour. Suppl. 56, 507-649 (1984)>
 =1984ApJS...56..507W

ADC_Keywords: X-ray sources

Mission_Name: HEAO

Abstract:

The HEAO A-1 X-Ray Source Catalog is a compilation of data for 842 sources detected with the U. S. Naval Research Laboratory Large Area Sky Survey Experiment flown aboard the HEAO 1 satellite. The data include source identifications, positions, error boxes, mean X-ray intensities, and cross identifications to other source designations.

Introduction:

The primary objective of the Naval Research Laboratory (NRL) Large Area Sky Survey Experiment (LASS) flown aboard the HEAO 1 satellite was to conduct an all-sky survey for the brightest X-ray sources in the energy range 0.25 to 25 keV. The instrumentation consisted of an array of large proportional counter modules with collimators of varying fields of view and with sufficient sensitivity to detect sources as faint as 0.25 muJy at 5 keV, assuming a Crab-like spectrum (1.1 muJy at 5 keV = 1 UFU for a Crab-like spectrum). Full sky coverage was achieved in the first 6 months of the mission by continuously scanning great circles perpendicular to the Earth-Sun line. The HEAO A-1 catalog results from the 6-month survey and, thus, covers the whole sky. For additional information concerning the NRL LASS instrument, the data analysis procedures, characteristics and limitations of the source data, and a discussion of X-ray source classes, the source publication should be consulted.

File Summary:

FileName	Recd	Records	Explanations
ReadMe	80	.	This file
sources.dat	303	842	The data

Byte-by-byte description of file: sources.dat

Bytes	Format	Unit	Label	Explanations
1- 10	A10	---	name	Source designation (1H)
12- 17	F6.2	deg	RAdeg	Right ascension 1950 in degrees
19- 20	I2	h	RAh	RA (B1950.0) hours
22- 23	I2	min	RAm	RA (B1950.0) minutes
25- 26	I2	s	RA s	RA (B1950.0) seconds
28- 33	F6.2	deg	DEdeg	Declination 1950 in degrees
35	A1	---	DE-	Declination sign
36- 37	I2	deg	DEd	Dec (1950.0) degrees
39- 40	I2	arcmin	DEm	Dec (1950.0) minutes
42- 43	I2	arcsec	DEs	Dec (1950.0) seconds
45- 50	F6.2	deg	GLON	Galactic longitude
52- 57	F6.2	deg	GLAT	Galactic latitude
59- 64	F6.2	deg	ELON	Ecliptic longitude
66- 71	F6.2	deg	ELAT	Ecliptic latitude
73- 78	F6.2	deg	RA1	Right ascension_1 (1)
80- 85	F6.2	deg	DE1	Declination_1. (1)
87- 92	F6.2	deg	RA2	Right ascension_2 (1)
94- 99	F6.2	deg	DE2	Declination_2 (1)
101-106	F6.2	deg	RA3	Right ascension_3 (1)
108-113	F6.2	deg	DE3	Declination_3 (1)
115-120	F6.2	deg	RA4	Right ascension_4 (1)
122-127	F6.2	deg	DE4	Declination_4 (1)
129-133	F5.3	deg2	area	Area of error box
135-141	F7.4	ct/cm2/s	flux	Flux (2)
143-148	F6.4	ct/cm2/s	e_flux	Flux error (2)
150-161	A12	---	name2	Alternate designation (X-ray) (3)
163-174	A12	---	name3	Alternate designation (X-ray) (3)
176-188	A13	---	name4	Alternate designation (X-ray) (3)
189-200	A12	---	name5	Alternate designation (X-ray) (3)
202-213	A12	---	name6	Alternate designation (X-ray) (3)
15-226	A12	---	name7	Alternate designation (X-ray) (3)
228-239	A12	---	name8	Alternate designation (X-ray) (3)
241-255	A15	---	name9	Alternate desig. (non-X-ray) (3)
257-271	A15	---	name10	Alternate desig. (non-X-ray) (3)
273-287	A15	---	name11	Alternate desig. (non-X-ray) (3)
289-303	A15	---	name12	Alternate desig. (non-X-ray) (3)

Note (1):

The source coordinates (center of error box) are given in degrees and in sexagesimal form. The subscripted right ascensions and declinations (right ascension_1-4, declination_1-4) give the positions of the 95 percent confidence error box surrounding each source. All positions are for equinox B1950.0.

Note (2):

The apparent intensity of the source in counts/sq.cm/s for 0.5 - 25 keV. The determination of the errors is described in Section III of the source reference (Wood et al. 1984). As explained in that paper, an intensity of 10^{*-3} counts/sq.cm/s, which is the limiting flux in the catalog, corresponds to $3.3 \times 10^{*-12}$ ergs/sq.cm/s in 2-10 keV, both for a Crab-like spectrum, meaning that 10^{*-3} counts/sq.cm/s in HEAO A-1 is equivalent to 0.20 UFU or to 0.22 μ Jy at 5.2 keV, again for a Crab-like spectrum.

Note (3):

The first seven fields (bytes 150-239) contain alternate designations of each source in other X-ray catalogs, while the last four fields are for non-X-ray cross identifications. Catalog identifications and references are given in Table 5 of the source paper. Cross identifications were selected according to certain criteria. For X-ray catalogs (4U, 2A, 1M, etc.), where error boxes of up to several degrees are sometimes reported, the cross reference is given whenever the other error box intersects the HEAO A-1 error box. Identifiers are also given in certain cases where boxes do not strictly intersect but are sufficiently close to suggest a possible relationship. The criterion used is that the separation between box centers must be less than the sum of the two largest dimensions. The designation XRS (not included in Table 5, but described in text) is from Amnuet, Guseinov, and Rakhimov (1979), which summarizes much of the older X-ray literature.

Non-X-ray cross identifications were made on several bases. Whenever an identification has been firmly established, for example, by a precise position from a modulation collimator or from the Einstein Observatory, it is always shown, but so are many additional tentative identifications. Some of these have been suggested by earlier work (in which case the earlier literature appears either in Table 5 or Table 6 of the source reference) and the remainder have been found by searching the non-X-ray catalogs listed by the authors in their Table 5. Additional information on selection criteria will be found on page 647 of the source reference.

Whenever an (R) appears in the last field, additional references and comments will be found in Table 6 of the source reference. Those entries are intended primarily to provide a sketch of the basic background and current state of knowledge concerning the sources, to direct users to further literature, and to clarify ambiguities. They are not intended to be a comprehensive bibliography and many references are omitted. A special effort has been made to provide cross references to other HEAO 1 literature wherever possible, since other HEAO 1 observations are simultaneous with and complementary to those in the catalog.

History:

The HEAO A-1 X-Ray Source Catalog was received on magnetic tape by the National Space Science Data Center on 20 July 1984 from Dr. Kent S. Wood of the Naval Research Laboratory. The tape was in VAX VMS BACKUP format with variable length logical and physical records, plus special control words (logical record length of each record in the first four bytes.) A program was written to convert the records to fixed length and the tape file was processed to disk storage on the IBM 3081 computer of the NASA Space and Earth Sciences Computing Center at GSFC. The format of the file was identical to Table 4 of the published catalog, meaning that there were 10 sources per group (page in the published catalog), separated by column headings and blank records, etc. All blank, text, and separator records were removed with an editor, leaving just four records per source. A format was designed that rearranged the data in logical order for a single record per source structure, and a program was written and executed to reformat the data. The advantages of the single record per source structure are that all records are entirely uniform and the catalog can be sorted and searched easily.

The original catalog contained the error box positions in both decimal and sexagesimal form. The latter data were omitted during the conversion in order to decrease the final record length, since the sexagesimal data can be reconstructed easily from the decimal positions given.

Acknowledgments:

Appreciation is expressed to Kent Wood for communicating about the catalog in 1986 and for supplying multiple copies of the source paper. Dr. Warren also thanks Dr. Wood for reviewing and commenting on a

draft version of this document.

The help of Jonathan McDowell of the Harvard-Smithsonian Center for Astrophysics is also gratefully acknowledged. Dr. McDowell requested a machine-readable copy of the catalog and made suggestions about the proposed format, including the elimination of the redundant error box positions in sexagesimal form.

The catalog was edited and the documentation prepared by Dr. Wayne Warren. It was translated from Script to ASCII and put in the current standard form by the undersigned.

References:

Annuel, P. R., Guseinov, O. H., and Rakhimov, Sh. Yu. 1979,
=1979ApJS...41..327A

Wood, K. S., Meekins, J. F., Yentis, D. J., Smathers, H. W., McNutt, D.
P., Bleach, R. D., Byram, E. T., Chubb, T. A., Friedman, H., and
Meidav, M. 1984, The HEAO A-1 X-Ray Source Catalog,
=1984ApJS...56..507W

(End) Nancy G. Roman [ADC/SSDOO] 08-May-1995

WHT
#7080

THE HEAO A-1 X-RAY SOURCE CATALOG

K. S. WOOD, J. F. MEEKINS, D. J. YENTIS, H. W. SMATHERS, D. P. MCNUTT,
R. D. BLEACH, E. T. BYRAM,¹ T. A. CHUBB,¹ AND H. FRIEDMAN
E. O. Hulburt Center for Space Research, Naval Research Laboratory

AND

M. MEIDAV
Tel Aviv University

Received 1983 September 6; accepted 1984 June 21

ABSTRACT

We present a catalog of X-ray sources detected with the NRL Large Area Sky Survey Experiment on the *HEAO 1* satellite. The catalog is derived from the first 6 months of data from *HEAO 1*, during which time one scan of the entire sky was completed. The text describes the instrument and data analysis techniques used for the survey.

Positions and intensities for 842 sources are cataloged, with a limiting flux of 250 nJy at 5 keV, or ~ 0.25 UFU. The catalog is more than 90% complete at a flux level equivalent to 1.5 μ Jy at 5 keV, for a Crab-like spectrum.

This catalog, more so than earlier ones done in X-rays, approximates a representative, instantaneous image of the sky in X-ray wavelengths, in that all sources are observed within a single 6-month interval, and epochs of observation for individual entries can be specified to within a few days. The intensity shown for a source is a mean value over the observing interval rather than an extreme value.

The catalog has been cross-referenced with published literature. Identifications based on coincidence in position are proposed for some of the sources for which previous work has established no firm identification. About one-half of the sources remain unidentified.

Subject heading: X-rays: sources

I. INTRODUCTION

The NRL Large Area Sky Survey Experiment (LASS) on the *HEAO 1* satellite, also referred to as the *HEAO A-1* Experiment, had as its primary objective the generation of an all-sky catalog of the brightest X-ray sources in the energy range from 0.25 to 25 keV. The instrumentation consisted of an array of large aperture proportional counter modules with collimators of varying fields of view. This array had sufficient sensitivity to detect sources as faint as 0.25 μ Jy at 5 keV, assuming a Crab-like spectrum (1.1 μ Jy at 5 keV = 1 UFU, for a Crab-like spectrum). The modules with the finest collimators ($1^\circ \times 0.5^\circ$) were not confusion-limited at the low end of this range.

Full sky coverage was achieved in the first 6 months of operation by continuously scanning great circles perpendicular to the Earth-Sun line. The present catalog is derived from those 6 months and thus covers the full sky. The uniformity of the catalog depends upon the exposure, defined as collecting aperture multiplied by accumulated integration time, achieved in various sky regions. Instrumental sensitivity improves as exposure increases, until the confusion limit set by the instrumental field of view is reached. The ideal sky coverage for the instrumental design and satellite scanning geometry would be to accumulate a sufficient minimum exposure everywhere such

that all sky regions would be uniformly limited by source confusion, and any remaining variations in exposure would not affect limiting sensitivity. Because some detector modules failed during the first 6 months, the flux limit for the present catalog in some sky regions is limited by exposure rather than confusion. The continued life of four of the original seven modules for an additional 11 months past their design goal meant that the ideal coverage was eventually achieved during the balance of the mission. Future addenda to the present catalog will be able to utilize the superior uniformity of the full mission sky exposure. The source list given here is at least 90% complete at a flux level equivalent to $\sim 1.5 \mu$ Jy at 5 keV for a Crab-like spectrum judging from the number versus flux curve and from known sources that do not appear in the list. The main causes for omission of sources brighter than 1.5 μ Jy are local imperfections in sky coverage or source confusion in the $1^\circ \times 4^\circ$ FOV scan modules, which serve as the principal source finders for the catalog. Thus a 5 μ Jy source might be missed if it were too close to another source brighter than 50 μ Jy. A later publication will utilize the $1^\circ \times 0.5^\circ$ modules to improve completeness in this respect. Allowing for these limitations, the all-sky catalog presented in this paper is the most uniform and comprehensive produced to date from a single instrument.

Section II provides a technical description of the *HEAO A-1* instrument. It is a more comprehensive description than

¹Also Bendix Field Engineering Corp.

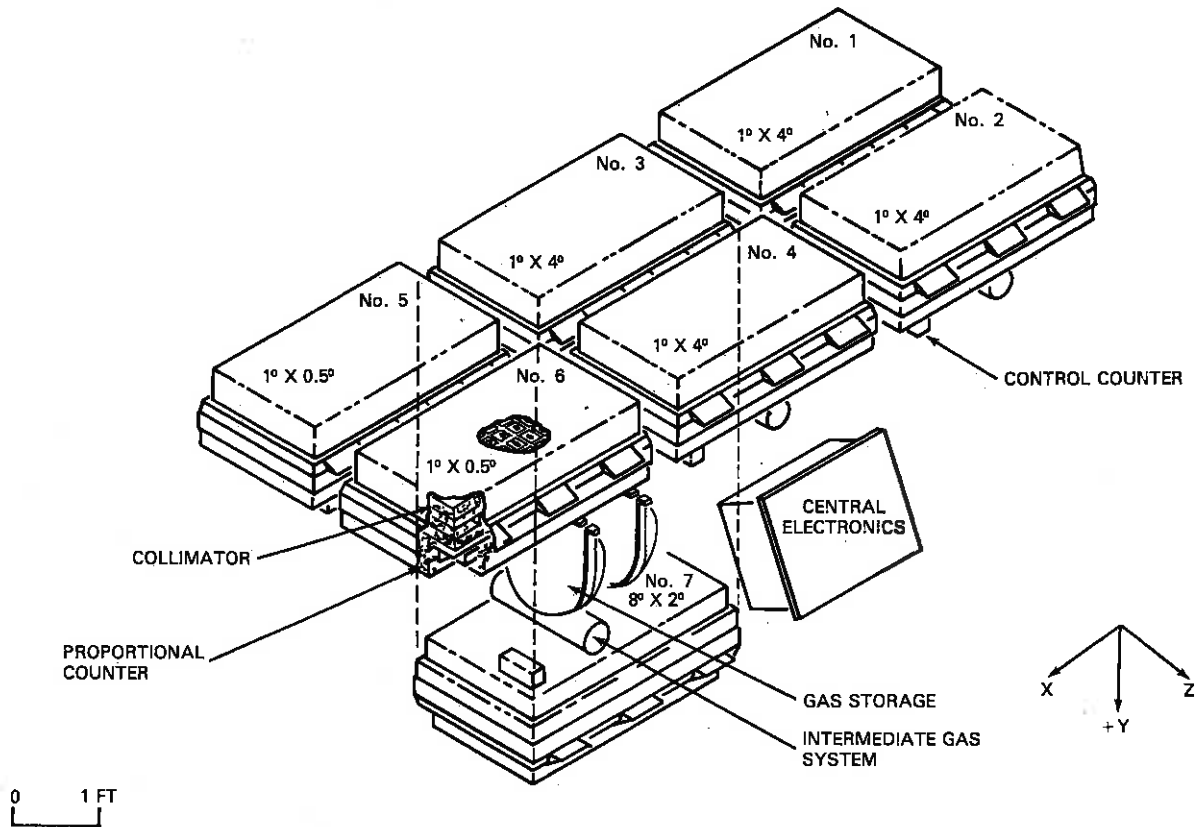


FIG. 1.—Schematic of the A-1 instrument as placed in the *HEAO 1* spacecraft

any that has appeared in previous publications and emphasizes aspects of the instrument which are important for understanding how the catalog was produced. Section III describes data analysis procedures used to extract source characteristics. Section IV introduces and describes the catalog tables. Section V is a brief discussion of source classes appearing in the catalog.

II. INSTRUMENT DESCRIPTION

a) Overview of the *HEAO 1* Instrument: Principal Subassemblies

The *HEAO 1* instrument was a modular assembly of seven thin-window proportional counters sensitive from 0.25 to 25 keV. Additional principal subassemblies of the instrument were a central electronics module, two ultraviolet stellar aspect sensors, and a central gas reservoir module.

The configuration of the A-1 instrument as mounted in the *HEAO 1* spacecraft is shown in Figure 1. Six of the seven X-ray sensor modules were placed on the $-Y$ side of the spacecraft, and the seventh on the $+Y$ side. The Z -axis of the spacecraft pointed toward the Sun; hence, the view directions of the seven A-1 sensor modules were roughly perpendicular to the solar direction. The exact alignment of sensor view directions is specified in Table 1; the effective collecting areas of the modules are also given there.

Data were formatted within the central electronics module of the A-1 instrument prior to storage on the *HEAO 1*

TABLE 1
X-RAY SENSOR VIEW DIRECTIONS AND OPEN AREAS

Sensor Module	View Direction ^a	Open Area (cm ²)
1, 2, 3, 4	$-Y$	1650
5	$-Y + 1/3^\circ Z$	1350
6	$-Y - 1/3^\circ Z$	1350
7	$+Y$	1900

^aRelative to spacecraft.

spacecraft tape recorder for later transmission. Two commandable standard formats were used, one having timing resolution of 320 ms and the other having 5 ms resolution. Essentially full-sky coverage was obtained in both formats; data taken in either mode are combined in summations used to produce the catalog.

b) X-Ray Sensor Modules

Each X-ray sensor module consisted of three main parts: (a) the grid collimator assembly, with heat shield; (b) the proportional counter; and (c) electronics and gas system assemblies mounted on the back of the counter. A cross-sectional view of the counter is shown in Figure 2. The proportional counter contained three layers of anode wires spaced 2 inches apart. Each layer of wires was read out independently. Over most of the energy range, the A layer (front layer) served

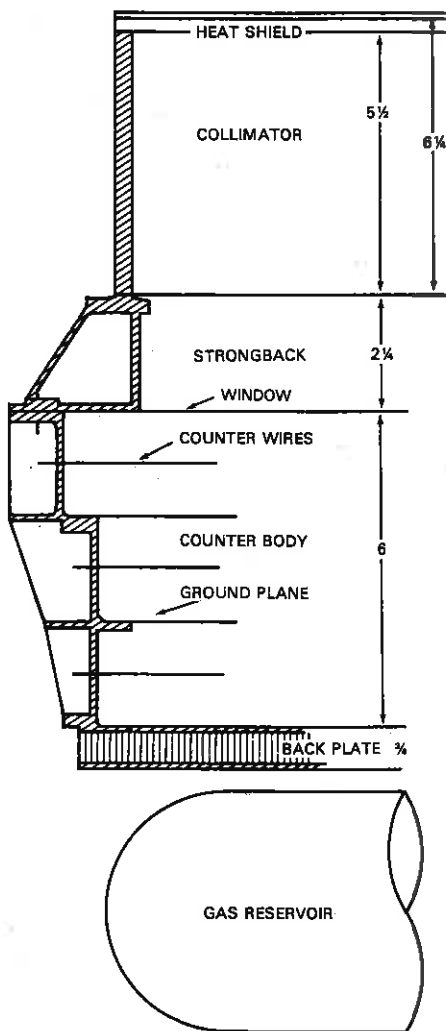


FIG. 2.—Cross sectional view of the sensor module, showing heat shield, front strongback, proportional counter, control counter, and gas tank.

as the X-ray sensor, and the B and C layers (middle and back layers, respectively) provided anticoincidence protection against charged particle events. For photon energies ≥ 10 keV (high gain) or ≥ 45 keV (low gain), added sensitivity was provided by the B layer, with the other two layers in anticoincidence. Anticoincidence protection was also provided on the ends and the sides of the A layer by additional background-counting anodes within the counter. (Protection against low to intermediate energy electrons was provided by magnets placed within the grid collimators.) The counter gas was a mixture of 22% methane and 78% xenon, at a nominal pressure of 2 psia (pounds inch⁻² absolute). Incoming X-rays reached the active gas volume by passing through a window of 2.5 μ m Mylar film; electrical conductivity of the inward surface was provided by a film of Nichrome, ~ 45 Å thick. The window was held in place by a stainless steel mesh which, in turn, was supported against the gas pressure within the counter by a rectangular cell stainless steel honeycomb strongback (window support structure). This honeycomb provided part of the X-ray collimation as shown in Table 2.

TABLE 2
COLLIMATION ANGLES

Sensor Module	Honeycomb Collimation Angles ^a	Grid Collimation Angles ^a	Resultant Collimation Angles ^a
1,2,3,4	8° × 4°	1° × 45°	1° × 4°
5,6	8° × 4°	1° × 0°5	1° × 0°5
7	8° × 8°	45° × 2°	8° × 2°

NOTE.—The first dimension is measured in the scan plane; the second, perpendicular to the scan plane.

^aOne-half full width.

c) Collimators

Above the honeycomb strongback, each counter had an additional multigrid collimator, which completed its field of view (FOV) as shown in Table 2. The grid collimators each consisted of a stack of etched molybdenum sheets interleaved with spacer frames. In order to prevent excessive heat loss or gain of the sensor modules while in orbit, a heat shield fabricated from 2 μ m Kimfol polycarbonate film and coated on its inner surface with 800 Å of aluminum was placed in front of each collimator. Incoming X-rays passed through this heat shield as well as the Mylar film, and the net transmission of the two layers determined the response to soft X-rays.

Prior to launch, the angular response of the collimators (grid and honeycomb in series) was estimated for each detector type by performing Monte Carlo simulations. From these simulations the net transmission at normal incidence and the relative angular response of each collimator assembly were determined. The simulations verified that the collimator response function could be factored into two components, $R_p(\theta)$ and $R_s(\phi)$, each a function of only one of the orthogonal angles measured from the two planes of symmetry of the collimators. Factorization was valid at the energies of interest, ≤ 25 keV. The symbols R_s and R_p refer to the response of the collimator in the scan direction and the direction perpendicular to the scan, respectively.

Figures 3, 4, and 5 give the responses R_s and R_p of the 1° × 4° collimators, 8° × 2° collimator, and 1° × 0°5 collimators, respectively. The curves are least squares fits of a cubic polynomial to the values determined by the Monte Carlo simulations.

After launch, data obtained from scans through the Crab Nebula were used to determine the angular response of the four scan sensor modules taken together (sensor modules 1, 2, 3, and 4). These four sensor modules were coaligned (see Table 1). Most of their data were added together by the spacecraft electronics prior to transmission to ground. The resultant angular response is shown in Figure 6. This experimental response agrees, essentially, with that shown in Figure 3, although there are small differences arising from slight misalignments of the four scan sensor modules with respect to one another.

d) Detection Efficiency

The X-ray detection efficiency for a module is shown in Figure 7. The two portions of the figure refer to two gain modes described below. Calculation of the efficiency takes into

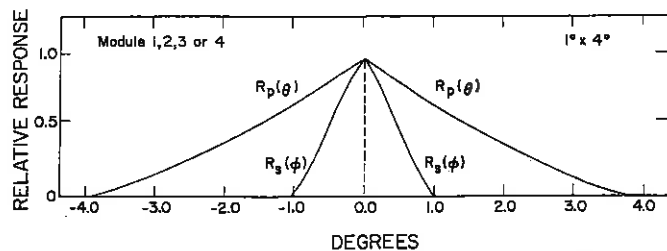


FIG. 3.—Angular response of a single $1^\circ \times 4^\circ$ sensor module (module 1, 2, 3, or 4). Here and in Figs. 4, 5, and 6, the total response is $R_s \times R_p$.

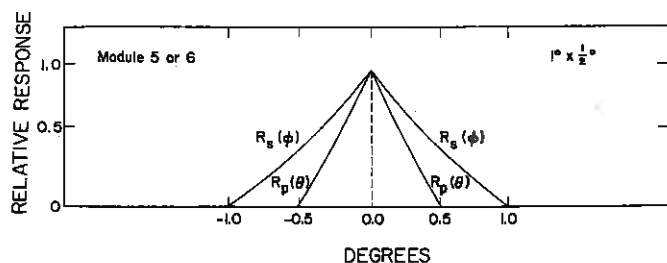


FIG. 5.—Angular response of a $1^\circ \times 1/2^\circ$ sensor module (module 5 or 6).

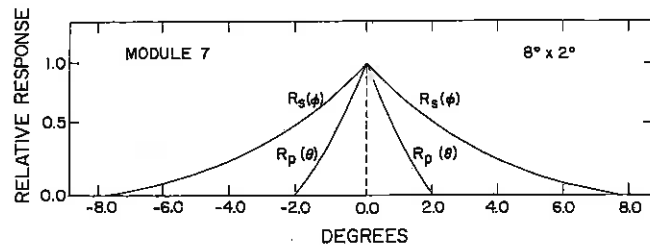


FIG. 4.—Angular response of the $8^\circ \times 2^\circ$ sensor module (module 7)

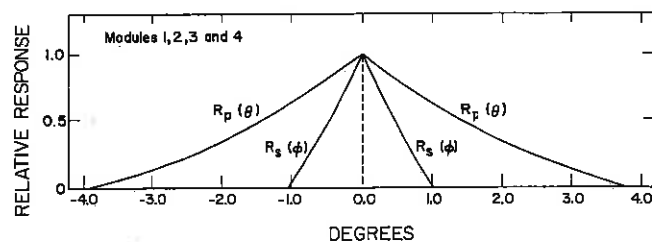


FIG. 6.—Composite angular response of the scar modules (modules 1, 2, 3, and 4).

account the effects of absorption in the gas, window, and heat shield. The self-anticoincidence of some X-ray events (arising when fluorescence X-rays are recorded in an adjacent counter layer) is also taken into account. Detection efficiency is defined as the likelihood of a photon of given energy being reported by the instrument, and it specifically includes discriminator effects.

e) Module Electronics

Except for differences in UV aspect sensor circuitry (present only on sensor modules 2 and 3), all sensor modules were essentially identical in their electronics. Each proportional counter included a set of prime data wires (A), secondary data wires (B), and background wires (C). Each set of wires had its own associated preamplifier, high-voltage filter, and decoupling network. For anticoincidence purposes, all B layer events were used for which energy deposition exceeded 2 keV (low gain) or 0.5 keV (high gain); B layer events that were not anticoincided were accepted as valid X-ray data whenever B layer energy deposition exceeded 50 keV (low gain) or 10 keV (high gain). The A layer data discriminators could be commanded to any of 16 levels. Typically, the A layer data discriminators were set to the lowest level, i.e., to record events when A layer energy deposition exceeded 0.5 keV (low gain) or 0.1 keV (high gain).

Integral to the back of each X-ray sensor module was a small auxiliary control proportional counter sharing counting gas with the main counter. It was excited by an internally mounted low-level radioactive source ($< 0.5 \mu\text{curies}$ of ^{55}Fe). This small counter could serve, when so commanded, as an

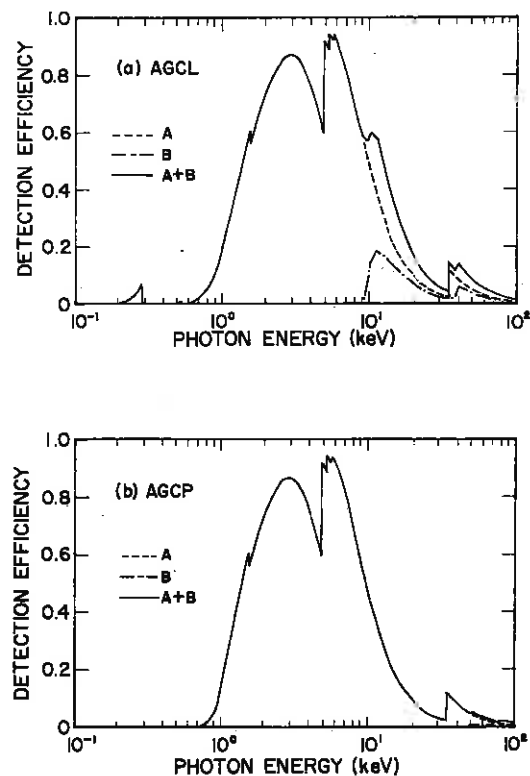


FIG. 7.—HEAO A-1 detector efficiency. Shown are the detection efficiencies (defined as the fraction of incident photons actually counted allowing for quantum efficiency, resolution and discriminator settings) for layer A, layer B, and for their sum, as a function of photon energy.

electronic component in a feedback loop, adjusting the operating voltage on the detector wires continuously so as to provide a constant gas gain despite density or composition changes in the counter gas.

Two commandable high-voltage modes were used for the bulk of the data collected. One of these (designated the "AGCL" mode) utilized the gain control feedback loop so as to set the ^{55}Fe 5.9 keV X-ray peak at 30% of full scale. The second mode ("AGCP") kept the voltage fixed at 1500 V and was equivalent to a comparatively low gain with the 5.9 keV peak at $\sim 6\%$ of full scale. A third controlled mode (with gain higher than the AGCL mode) was available but was used only rarely, and never for data contributing to the catalog.

After processing by anticoincidence logic and discriminators, data pulses were passed to a 256 channel linear analog to digital converter (20 mV per channel, 5.1 V full scale) which digitized the height of the pulses. These signals were sent to the central electronics module for further processing, described below.

In-flight calibrations were of two types, ramp calibration, which checked analog-to-digital conversion and amplifier linearity, and active calibration with ^{55}Fe sources, which checked the system response to 5.9 keV photons.

f) Central Electronics and Telemetry

The central electronics (CE) module provided the electrical interfaces between the A-1 instrument and the spacecraft. This module received, processed, and formatted data from the sensor modules in preparation for storage by the spacecraft.

The X-ray pulses from each sensor module underwent pulse-height analysis (PHA) into 256 linear channels and then were presented to the CE. There the 256 channels were compressed to 16, using nonlinear sorters as shown by the energy threshold breakpoints in Table 3. One of the 16 channel sorters accumulated the data from sensor modules 1, 2, 3, and 4 taken together, these being the modules with co-aligned $1^\circ \times 4^\circ$ fields of view. In contrast, each of the sensor modules 5, 6, and 7 had its own 16 channel sorter. In addition, the telemetry format allowed for one further spectrum to be transmitted. This spectrum used a 40 channel nonlinear sorter analogous to the 16 channel sorters just described, and it could accept inputs from any of the modules, singly or in combination. Count accumulations from all sorters, as well as the total count from each sensor module, were processed by quasi-logarithmic scalars. The data, together with housekeeping information, were stored in an onboard tape recorder in one of two standard formats and subsequently were transmitted to the ground.

Data used in preparation of the catalog consisted either of 320 ms count accumulations from the scan module 16 channel sorter or 640 ms count accumulations from the 40 channel sorter. The latter was used when the instrument was in the 5 ms telemetry format. PHA bins from the 40 channel sorter were, for these purposes, added together so as to be identical to bins from the 16 channel sorter, so that Table 3 applies to both cases. Further details on the instrument may be found in Friedman (1979). An additional capability for timing of X-ray events with resolution as fine as a few microseconds is de-

TABLE 3
16 CHANNEL SORTER LOWER LEVEL BREAK POINTS

Sorter Channel	Linear Channel	Low Gain ^a (keV)	High Gain ^b (keV)
0.....	0	0 ^c	0 ^c
1.....	2	0.79	0.15
2.....	3	1.18	0.23
3.....	4	1.57	0.31
4.....	6	2.36	0.46
5.....	8	3.14	0.61
6.....	12	4.71	0.92
7.....	16	6.29	1.22
8.....	24	9.43	1.84
9.....	32	12.57	2.45
10.....	48	18.86	3.67
11.....	64	25.14	4.90
12.....	96	37.72	7.35
13.....	128	50.29	9.80
14.....	192	75.43	14.69
15.....	255	100.18	19.52

^a"AGCP" gain mode, 5.9 keV in 15th linear channel

^b"AGCL" gain mode, 5.9 keV in 77th linear channel.

^cLower limit depends upon commanded discriminator level.

scribed in Meekins *et al.* (1984); this feature is not relevant to the catalog.

g) Performance History and Cumulative Sky Exposure

During the mission, it was discovered that a reset problem existed in the module electronics which limited the determination of X-ray source spectra. When an X-ray event was recorded in layer A or B, it was found that the pulse height reported was not necessarily the pulse height produced by absorption of the X-ray photon. The pulse amplitude analyzed was the larger of the current X-ray event or the pulse height (charge) held in the electronics circuitry. If the preceding event had been an X-ray event, proper reset occurred and the charge held was zero; but if the preceding event had been a coincidence event, reset failed to occur and the charge held was the charge from the coincidence event. The number of pulses reported was a true count of the number of X-ray events, but the pulse height distributions were contaminated by the charged particle spectrum to a degree dependent upon both the X-ray rate and particle event rate. Contamination was more serious for faint sources than for bright ones.

On 1977 September 22, repetitive, short-duration noise bursts were found in data from sensor module 2 resembling continuous discharge. On the following day, the same condition appeared in the data from sensor module 1. All sensor modules were immediately turned off and vented. On 1977 September 26, sensor modules 3, 4, and 5 were turned back on at the lowest possible operating voltage, i.e., the AGCP gain mode. It was anticipated that this reduced high voltage would extend the life of the modules if high-voltage breakdown had been the cause of the noise bursts. On 1978 January 26, sensor module 4 failed in a manner similar to that of the failures of sensor modules 1 and 2 above.

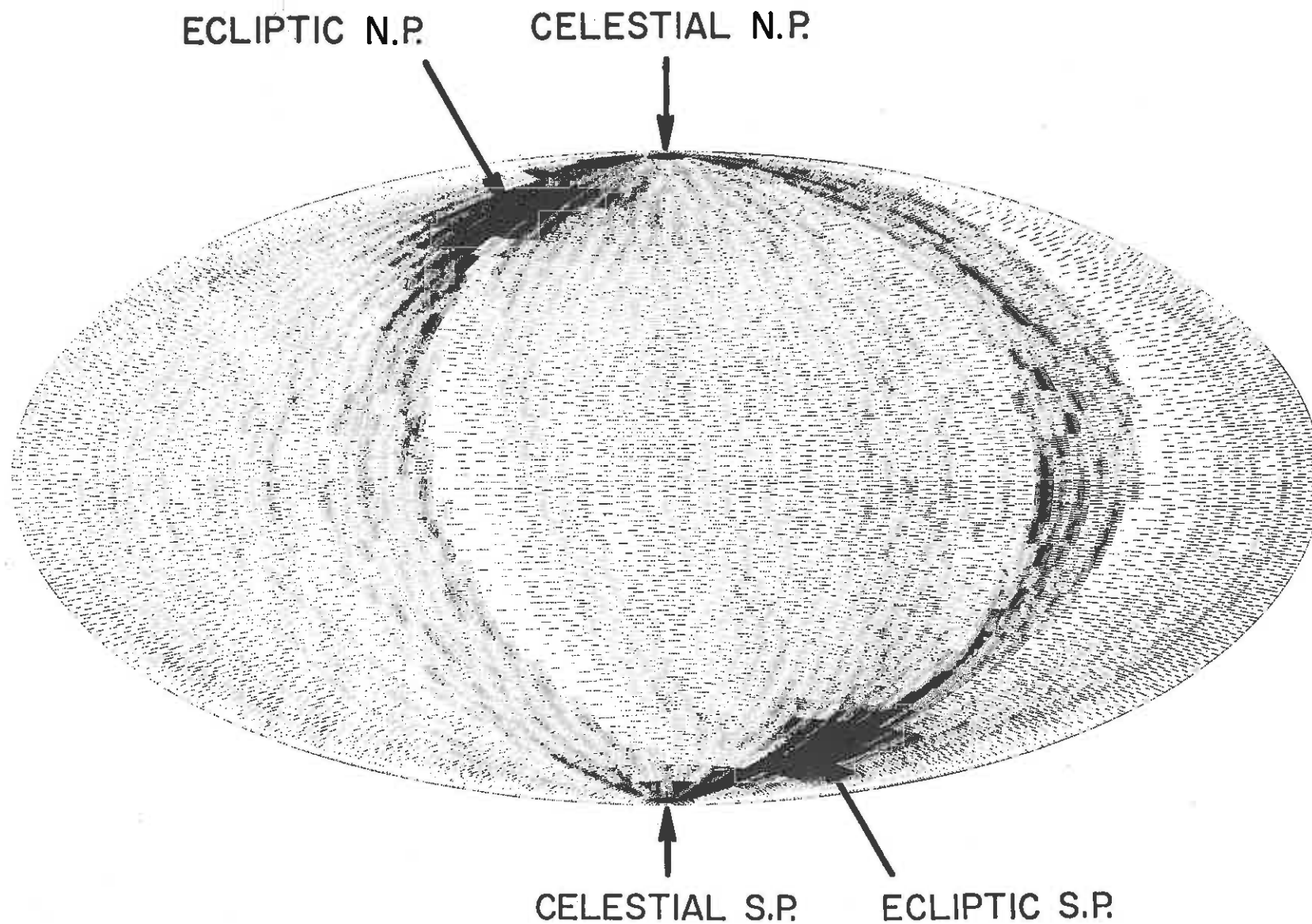


FIG. 8.—Sky exposure for first 6 months. The gray scale plot shows exposure ($= \text{area} \times \text{time}$) accumulated on each sky bin. The display is an Aitoff projection in celestial coordinates. The two ecliptic poles appear as regions of very high exposure.

The malfunctions on 1977 September 22 and 1977 September 26 resulted in decreased sky exposure in the regions being scanned on those dates, an effect largely compensated by the coverage available on the dates immediately preceding and following. In addition, the detectors were shut down for most of the time on 1978 February 10–11 and again on 1978 February 14, in order to minimize risks to the hardware associated with intense solar activity that was then occurring. The correlation of these dates of reduced coverage with regions on the sky may be made by a procedure described in § III.

Because of the extension of the *HEAO 1* mission beyond its planned 6 months, the X-ray sky survey eventually exceeded the original goals both in terms of total exposure (area \times time) and in terms of the total time span for which each sky element was monitored. Sky exposure achieved in the first six months is mapped in Figure 8, in celestial coordinates.

III. DETERMINATION OF X-RAY SOURCE CHARACTERISTICS

a) Overview of the Catalog Processing

In order to determine source positions and intensities for the catalog, the detector readouts (in which count accumulations are given as a function of time) must first be combined with the aspect solution (provided by NASA and accurate to $\pm 0^{\circ}01$) in a data summation scheme. Data are summed in bins according to where they fall in the roll of the spacecraft. These summations then are fitted using nonlinear least squares fitting routines. *HEAO 1* spacecraft motion was controlled to make this technique comparatively simple: the satellite spin axis was kept pointed toward the Sun and held at one position for 12 hr, after which it was advanced $\sim 0^{\circ}5$. This means that scan planes are all normal to the ecliptic plane (i.e., follow meridians of constant ecliptic longitude), intersecting at the ecliptic poles (see Fig. 9 for this geometry). It also means that, over most of the sky, a particular source appears at almost exactly the same phase angle in the scan on each day that it is seen. Lines of position determined on successive days are

therefore nearly parallel. The method of reducing source error regions by means of intersecting lines of positions (used, e.g., in the *Uhuru* catalogs) is ineffective, and other techniques must be used to locate a source. Two such techniques are used, one based on the $1^{\circ} \times 4^{\circ}$ modules alone and the other utilizing the $1^{\circ} \times 0^{\circ}5$ modules in conjunction with the $1^{\circ} \times 4^{\circ}$ modules. The stages of source localization will now be described in detail.

b) Data Summations

The first phase of data reduction is a program that unpacks data and moves them to disk storage, simultaneously accumulating a time-averaged value for the direction of the Z-axis (spin axis) for the 12 hr interval. The coordinate system used for data summation is defined as having its pole in the direction of this same spin axis and its zero of longitude at the northward crossing of the ecliptic plane. This is designated the "scan" coordinate system, with coordinates scan longitude and scan latitude. The angular distance along the scan (i.e., the phase of the spacecraft roll) is scan longitude. The system is redefined for each advance of the spin axis. Deviations of actual spacecraft motion to either side of the nominal scan plane defined by the time-averaged Z-axis (in the scan latitude direction) are controlled so as not to exceed $0^{\circ}5$.

The second phase is a program that reads data back from the disk and bins them according to scan longitude. Two separate arrays of bins are maintained: one for counts as a function of scan longitude, and the other for exposure (equal to detector collecting aperture multiplied by dwell time in the angular range covered by the bin), also as a function of scan longitude. Both quantities are binned to $0^{\circ}1$, i.e., there are 3600 bins in the complete roll. Observed counts, which are read out every 320 ms (during which time the scan nominally advances $0^{\circ}06$), are fractionally rebinned according to the portion of time spent in each $0^{\circ}1$ scan longitude bin. Data are combined into five PHA bins, initially, but for source-fitting purposes, several of these PHA bins are summed together. The final product resulting from the second phase is a number of

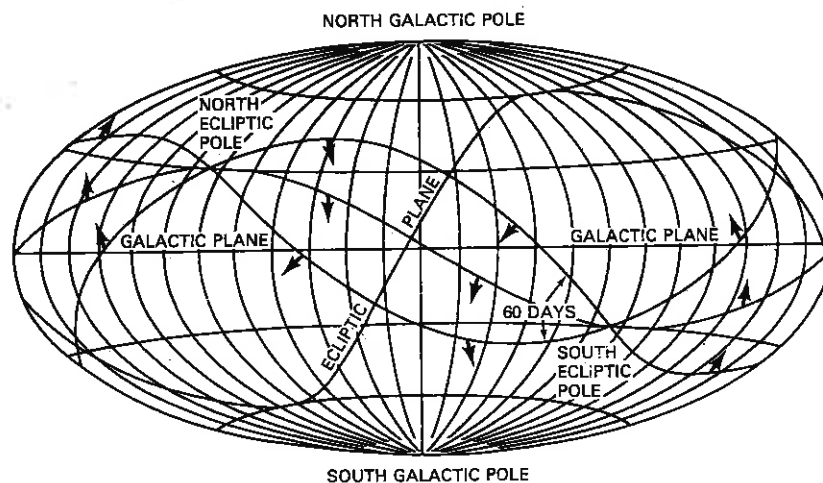


FIG. 9.—*HEAO 1* scan geometry. All scans run normal to the ecliptic (because the spin axis follows the Sun) and intersect at the ecliptic poles. Arrows indicate how the scan plane advances daily. The plot is in galactic coordinates.

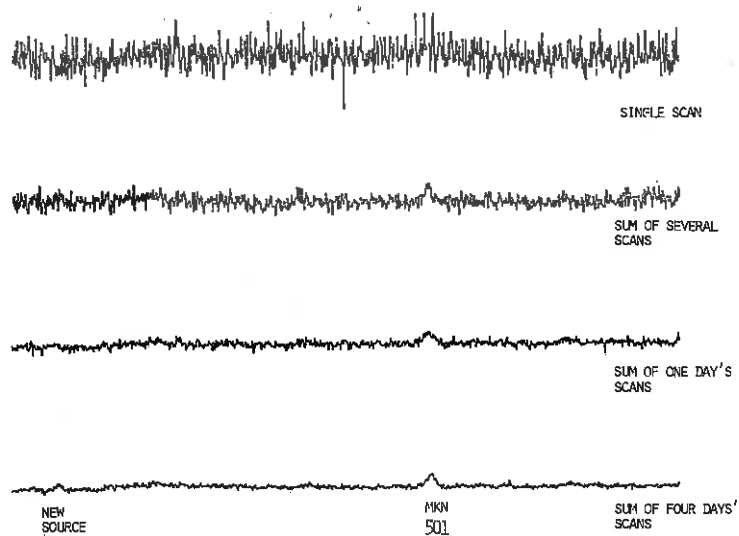


FIG. 10.—Scan summation. This shows enhancement of signal-to-noise ratio in a selected group of PHA channels as scans are summed. (The vertical scale is *fixed* in counts $\text{cm}^{-2} \text{s}^{-1}$; hence sources stay at fixed height while noise level decreases.)

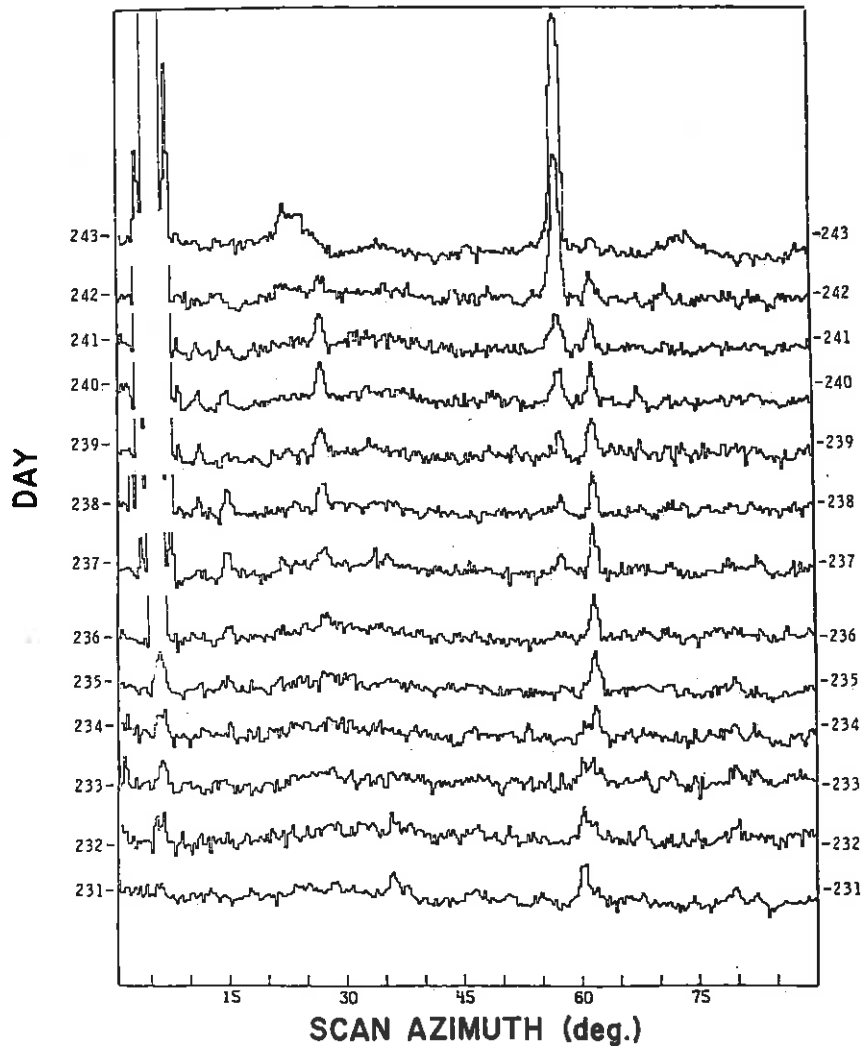


FIG. 11.—1 day scan summations. Each day represents an independent summation. These sums and the 4 day sums are used for first stage fitting, as described in § II.

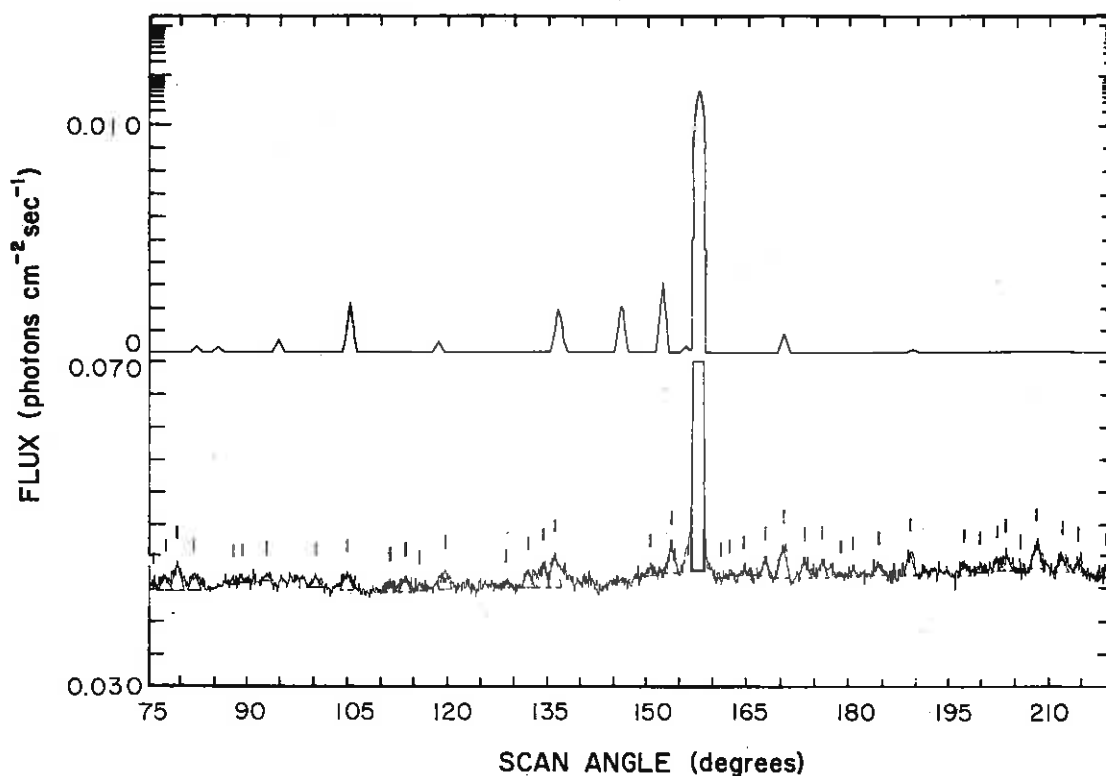


FIG. 12.—4 day sum segment, with superposition of first-stage fits is shown at the bottom. The upper portion of the figure shows predicted source positions and intensities based on literature published prior to *HEAO 1*.

sets of scans suitable for summation, each set covering ~ 12 hr, the interval over which the spacecraft spin axis is fixed. Scans are then added in register with one another to enhance the signal-to-noise ratio; the counts and exposure arrays are added separately. (The enhancement obtained in this way is illustrated in Fig. 10, which displays fluxes, or counts divided by exposure). Scans are summed first over 12 hr intervals, and the 12 hr summations are further summed so as to achieve greater sensitivity. Sets of 1, 2, and 4 day summations are produced for the full sky (see Fig. 11). Further summation is possible, but proves useful only at very high ecliptic latitudes. Fine collimator module data as well as those from the scan modules are summed in this manner.

c) Source Localization

These data summations are now suitable for source fitting. First, one fits each of the 4 day summations with a "source search" routine that makes no presumptions as to where it will encounter significant excess flux. The first pass establishes a library of potential source locations in the scan longitude direction using all available 4 day summations. Figure 12 shows an example. (The 4 day summations are redundant, i.e., the first one contains days 1-4, the second one contains days 2-5, and so on, but fits to them are used only for source discovery, not for error box determination.) A second pass using a similar routine is now made on the 1 day sums, which are independent of one another. On this pass, the routine has access to the library of potential locations established on the

first pass; if no excess flux is found at a location, a fit is nevertheless forced and an upper limit is obtained. The redundant fitting of 4 day summations means that the library of potential locations is highly complete. A source may occasionally be missed on 1 day, but it is rare for it not to be in the library of potential locations.

The fitting routine allows two free parameters for each source, intensity and position. It is assumed that the count in the i th bin of the data summation can be represented as

$$C_i = B_i + I_j R_s(\rho_i - \phi_j), \quad (1)$$

where C_i is the count in the i th bin, I_j is the intensity of the j th source and ϕ_j is its position, and R_s is collimator response in the scan direction (see § II) and is a symmetrical function of the difference between ϕ_j and the bin position, ρ_i . The quantity B_i is the quadratic fit to background, valid locally over 20° of scan longitude.

A nonlinear least-squares fit of the polynomial collimator response function (R_s) to the data provides source intensities and positions as error ellipses in the two-dimensional parameter space. These may be conceptualized as those ellipses that best approximate the 1σ confidence contour in χ^2 . Because errors are characterized in this way, it is possible to propagate them formally through further fitting in order to determine error boxes. This is done in two ways. One method uses only the fits to the scan module data, while the other also employs fits to the fine collimator modules. In the routines just de-

scribed, fits to fine collimator summations are forced at all scan module fit positions.

In the fitting scheme based on the scan modules alone, a second-stage least-squares fit is used to establish the source position in the direction perpendicular to the scan, i.e., scan latitude. The second fit takes as inputs only the fits obtained in the first stage; data summations are not presented directly to the second-stage fitting routine. (Hereafter, first-stage fits are called "sightings.") The second-stage fit routine first seeks regions where there are several sightings that may correspond to a single source. Since the collimator extends 8° in scan latitude (full width zero response), and since the scan plane advances 1° each day, a source on the ecliptic plane remains visible for ~ 8 days, yielding up to eight sightings. Sources at higher ecliptic latitudes remain visible for longer periods and yield more sightings.

The second-stage fit determines three parameters characterizing the source, two for position and one for intensity. The position error box is a rectangle that contains the 95% confidence contour interval obtained when the error ellipsoid is projected onto the two-dimensional position subspace of the parameter space. The method assumes that the source maintains constant brightness over the interval of observation. An error box of this kind is referred to as a "constant intensity error box," and it is obtained by fitting the daily intensities to the collimator response function, R_p , in the direction perpendicular to the scan. This is done by a least squares fit in which the source intensity and position are varied, intensity and scan longitude for each sighting are calculated, and χ^2 is minimized (see Fig. 13).

The other second-stage fitting technique utilizes both the scan ($1^\circ \times 4^\circ$) and fine mapping ($1^\circ \times 0.5^\circ$) modules, and yields a type of error box, henceforth referred to as a "fine collimator error box," that is in many ways superior to the constant intensity error box. Each scan module detection of a source by the first-stage fit routine establishes a line of position on the sky whose width (in the scan longitude direction) is defined by 95% confidence contours of the fit and whose length (in the scan latitude direction) is the 8° full width at zero response of the collimator. The simultaneous fits to the fine collimator module summations (forced in the first-stage fitting) are now used to truncate one of these lines of position so as to decrease its length. Since the fine collimator FOV lies entirely within the central portion of the larger FOV of the scan modules (see Tables 1 and 2), a detection in the former is made only when the source is near peak response in the latter. On adjacent days, the source may be detected in the scan modules but not in the fine collimator modules, since it lies outside their FOV. The strongest positive detection in the fine collimator from a group of sightings can thus be used to constrain the source position to that part of the scan module line of position falling within the fine field of view. Allowance of an additional $\pm 0.5^\circ$ in scan latitude is made, which is the tolerance in the spacecraft attitude control for perturbations of the spin axis. To summarize, the error region reported in the catalog for a fine collimator error box is the scan module 95% confidence line of position truncated at points $\pm 1^\circ$ from the center of the fine collimator FOV. The strongest detection in the fine collimator is used for this purpose. The intensity of the source reported

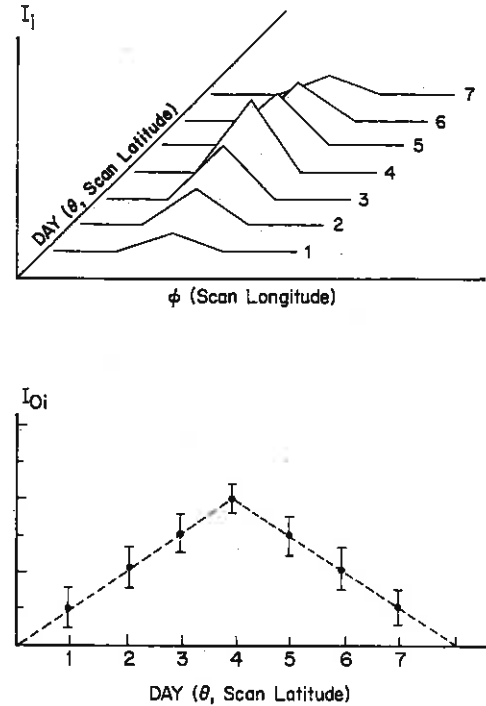


FIG. 13.—Visualization of constant intensity second-stage fit technique. *Top*: Representation of variation of source intensity over successive days (compare actual data in Fig. 10.) *Bottom*: By fitting $R_p(\theta)$ to first-stage fits and scan latitudes, source localization in the r -direction is obtained.

in this type of error box is that detected by the scan modules on the day when the source is also seen in the fine collimator modules.

Fine collimator error boxes require no assumptions about source constancy and thus are used in preference to constant intensity boxes whenever source variability is suspected. The fine collimator module detection is a second, statistically independent, detection of the source. Use of it minimizes the risk that the position is affected by source confusion, since the fine collimator modules are confusion free well below the catalog limit. Fine collimator error boxes are not available in every case because some sources are too faint to be seen with high statistical significance by the fine collimator modules or because fine mapping module coverage is incomplete near the date when the source transits in the FOV.

A third type of fit is used in the catalog for certain very bright sources with well-determined positions. These sources are bright enough that positions obtained for them are sensitive to small systematic effects, which can be thought of as misalignments of the modules with respect to the spacecraft coordinate system. The fit shown in the catalog in these cases is performed by fixing the source at its known position and varying only its intensity to minimize χ^2 . Thus, the source is shown in the catalog at its known position with an error of 0.0 deg^2 , and with an intensity which is its best fit value during the time when it was in view.

The known positions of these same sources were, however, first used as standards with which to determine and correct for

the collimator misalignments. The best-fit misalignment corrections were then retroactively applied to *all* fits used in the catalog, including those for the standard sources. The misalignments detected can be represented as a rotation about the spacecraft spin (Z) axis (which exhibits itself as a slight offset of the measured source position in the scan longitude direction in all detections) and another, smaller, rotation about the module look direction ($-Y$ axis) (which manifests itself as an additional scan longitude offset that varies in a regular manner from day to day, depending on the scan latitude of the source). Any misalignment with respect to the remaining axis proved undetectable. The misalignments could be measured with any single strong source such as Sco X-1 or the Crab Nebula, but the use of a larger ensemble (~ 30) of standard sources permitted a search for long-term variations in the corrections and other systematic effects. No such variations were identified in this search. Correction for misalignments is accomplished by modifying the scan longitude of the sighting when it is used by second-stage fitting routines. The increase in the error box width in the scan longitude direction as source brightness decreases means that these corrections become of diminishing importance for faint sources, i.e., statistical errors become more important than systematic ones.

In all of the second-stage fitting routines, provision is made for elimination of sightings which are judged to be affected by the confusion with nearby sources. In the great majority of cases there is no difficulty obtaining enough unconfused sightings to permit determination of the catalog entry, but it sometimes happens that two sources are so confused that one or both of them fail to appear. We estimate that, over most of the sky, this effect accounts for less than 5% incompleteness in the catalog down to a level of 6×10^{-3} counts $\text{cm}^{-2} \text{s}^{-1}$. More severe incompleteness is likely in the galactic bulge, but it is difficult to quantify. Over most of the sky, greater incompleteness results from imperfections in sky exposure than from confusion. In future refinements to the catalog, greater use will be made of the data from the fine collimator modules and from the later parts of the mission in order to reduce both sources of incompleteness.

Because of the regular *HEAO 1* scan pattern, there is a simple correspondence between the ecliptic longitude of the source and the date when it is in view, with transit occurring when the ecliptic longitude of the Sun differs from that of the source by 90° . Therefore, each catalog entry has an epoch good to about ± 4 days except at the highest ecliptic latitudes, and the full range of these epochs is 6 months, from 1977 August 15 to 1978 February 15. The epoch is calculable as just described from the data in Table 4. The display of the catalog (Fig. 14 [Pl. 20]) is thus a representative near-instantaneous sample of the X-ray sky. Since all intensities are best fits for their epochs rather than extreme values, some bright sources from our Galaxy stand out somewhat less strongly than in the corresponding fourth *Uhuru* catalog display (Fig. 4 of Forman *et al.* 1978), where maximum values were used instead. A noteworthy instance of this effect is the entry for Hercules X-1, which made a transition from its "off" to its "on" state while in the field of view, although it was detectable in both states. It thus appears as a substantially lower flux in the *HEAO A-1* catalog than in the *Uhuru* catalog.

d) Acceptance Criteria

Acceptance criteria for the catalog have been adopted to ensure not only the statistical significance of the excess flux in a region but also to exclude as fully as possible the effects of source confusion and transient effects of either instrumental or celestial origin. Accordingly, the basic requirement is that a source must have at least three independent detections at 3σ significance in either the scan modules or the modules with fine collimators. Furthermore, it is required that the flux measurements in the fine collimator modules be consistent with the cataloged flux, i.e., either a direct confirmation or a lack of coverage at the required date. For sources fainter than ~ 0.002 counts $\text{cm}^{-2} \text{s}^{-1}$ only marginal detections are expected in the fine collimator modules, and this condition does not apply. The requirement for three independent detections in 1-day summations necessarily excludes transient sources whose duration is less than a day.

IV. THE CATALOG

a) Positions and Intensities

The positions and intensities for 842 sources, as derived by methods outlined in the preceding section, are given in Table 4. Table 4 further provides cross references to other X-ray catalogs and to non-X-ray counterparts. These have either been established or suggested by earlier work or are proposed here on the basis of coincidence with the *HEAO A-1* position. The latter identifications have been found by searching other comprehensive catalogs, those shown in Table 5. For many of the entries in Table 4, substantial additional information concerning the source exists in the published literature. Table 6 complements Table 4 with brief summaries of current understanding in these cases. The remainder of this section is a detailed description of Tables 4 and 6.

In Table 4 the first column "CATALOG ENTRY," gives the 1H catalog designation. The name is "1H" followed by right ascension in hours and minutes, then followed by declination in degrees and tenths of a degree. The second column, "POSITION RA, DEC" denotes the (1950.0) right ascension and declination for the center of the error box. The upper two entries are right ascension and declination in degrees and decimal fractions of a degree. The lower two are the same values expressed in hours, minutes, and seconds for right ascension and degrees, minutes, and seconds for declination. The third column, "GAL, ECL," gives the center of the error box in galactic longitude and latitude (upper pair) and ecliptic longitude and latitude (lower pair), for 1950.0. The next four columns, "ERROR BOX, RA, DEC," specify the four corners of the 95% confidence error box in right ascension and declination. The notation is the same as that used to specify the center (as in the second column). The eighth column, "AREA," is the solid angle enclosed by the error box in square degrees. The ninth column, "FLUX, ERROR," gives the apparent intensity of the source in counts $\text{cm}^{-2} \text{s}^{-1}$ for 0.5–25 keV and its error as determined by the methods of § III. The final columns, "IDENTIFICATION," give identification of the source with other cataloged objects.

TABLE 5
 CATALOGS USED IN SEARCHING ERROR BOXES

Catalog	Source
X-Ray Catalogs	
Fourth <i>Uhuru</i> catalog	Forman <i>et al.</i> 1978
First <i>Ariel 5</i> X-ray catalog	Seward <i>et al.</i> 1976
Second <i>Ariel 5</i> X-ray catalog	Cooke <i>et al.</i> 1978
<i>HEAO A-2</i> hard X-ray catalog	Marshall <i>et al.</i> 1979
CGS catalog	Bradt, Doxsey, and Jernigan 1979
1M catalog	Markert <i>et al.</i> 1979
2S catalogs	Bradt 1978; Dower <i>et al.</i> 1978; Apparao <i>et al.</i> 1978; Jernigan <i>et al.</i> 1978; Doxsey <i>et al.</i> 1977a, b; Bradt <i>et al.</i> 1977; Jernigan <i>et al.</i> 1977
Radio, Infrared, and Gamma-Ray Catalogs	
3C radio catalog	Bennett 1962
Radio sources with optical identifications	Veron and Veron 1974
IR sources (2 μm)	Neugebauer and Leighton 1969
AFGL IR survey	Price and Walker 1976
<i>COS B</i> γ -ray sources	Masnou <i>et al.</i> 1977
Galactic/Stellar Catalogs	
Supernova search	Kowal <i>et al.</i> 1974
Supernova remnants	Ilovaisky and Lequeux 1972
Supernova remnants	Clark and Caswell 1976
Globular clusters	Arp 1965
Early-type stars with emission lines	Wackerling 1970
Variable stars	Kukarkin <i>et al.</i> 1970
White dwarfs	Luyten 1970
Stars at distances under 22 pc	Gliese 1969
Flare stars	Pettersen 1976
Catalogs of nebulae	Dreyer 1895, 1908
Extragalactic Catalogs	
Bright galaxies	de Vaucouleurs 1964
Compact and bright nucleus galaxies	Fairall 1970
Atlas of peculiar galaxies	Arp 1966
Markarian galaxies	Markarian 1974
Distant rich clusters	Abell 1958
Southern clusters of galaxies	Klemola <i>et al.</i> 1969; Duus and Newell 1977
Revised NGC catalog	Sulentic and Tiffi 1973
BL Lac objects	Stein, O'Dell, and Strittmatter 1976
BL Lac objects	Weiler and Johnston 1980
Quasars	Burbidge, Crowne, and Smith 1977

An intensity of 10^{-3} counts cm^{-2} s^{-1} in the ninth column, which is the limiting flux in the catalog, corresponds to 3.3×10^{-12} ergs cm^{-2} s^{-1} in 2–6 keV or, 4.78×10^{-12} ergs cm^{-2} s^{-1} in 2–10 keV, both for a Crab-like spectrum. This means that 10^{-3} counts cm^{-2} s^{-1} in *HEAO A-1* is equivalent to 0.20 UFU or to 0.22 μJy at 5.2 keV, again for a Crab-like spectrum. These calibration factors have been established by fitting the Crab Nebula at various elevations in the collimator, correcting the measured fluxes for instrumental dead time and collimator response, and comparing the mean flux so derived with the known spectrum of the Crab Nebula folded through instrumental responses. The conversion has also been checked on a sample of bright clusters of galaxies comparing the flux shown in the table in the ninth column with that given in the fourth *Uhuru* catalog (Forman *et al.* 1978).

The cross reference and identifications shown in Table 4 have been selected according to certain criteria. For X-ray catalogs (such as the 4U, 2A, and 1M catalogs) where error boxes up to several square degrees are sometimes reported, the cross reference is given whenever the other error box intersects the *HEAO A-1* error box. It will also be shown in certain cases where boxes do not strictly intersect but are sufficiently close to suggest a possible relationship. The criterion used here is that the separation between box centers must be less than the sum of the two largest dimensions. Few of the X-ray cross references are of this nonintersecting type. This procedure is conservative in that it reports the other catalog entry if it is remotely plausible. The designation "XRS" from the catalog of Amnuel Guseinov, and Rakhamimov (1979), which summarizes much of the older X-ray literature, also appears in some cases.

TABLE 4
X-RAY SOURCE POSITIONS AND INTENSITIES

CATALOG ENTRY	POSITION		ERROR BOX					FLUX ERROR	IDENTIFICATIONS	
	RA DEC	GAL ECL	RA DEC	RA DEC	RA DEC	RA DEC	AREA		X-RAY	NON X-RAY
1H0003+200	.80	108.63	359.78	1.72	1.83	359.90	.520	.0028	4U 0005+20 XRS00058+200	Mkn 335
	20.01	-41.31	19.71	20.55	20.31	19.47		.0006		
	00 03 12	8.97	23 59 07	00 06 51	00 07 19	23 59 35				
	20 00 43	17.98	19 42 31	20 32 45	20 18 33	19 28 23				
1H0007+731	1.91	119.97	359.79	3.75	4.22	.24	.324	.0054	4U 0000+72 XRS00000+726	CTA 1
	73.17	10.81	72.39	74.03	73.93	72.30		.0007		
	00 07 37	53.40	23 59 10	00 15 00	00 16 52	00 00 57				
	73 10 11	60.96	72 23 08	74 01 39	73 55 49	72 17 49				
1H0008-745	2.21	306.60	.11	3.25	4.14	1.06	.479	.0049		STR0000-751?
	-74.59	-42.53	-75.28	-73.76	-73.88	-75.42		.0010		
	00 08 51	305.36	00 00 27	00 13 01	00 16 32	00 04 14				
	-74 35 22	-62.69	-75 16 42	-73 45 27	-73 52 57	-75 24 58				
1H0010-515	2.62	317.15	1.20	3.81	4.01	1.39	.424	.0036		STR0012-515?
	-51.53	-64.80	-52.02	-50.86	-51.03	-52.19		.0007		
	00 10 29	335.33	00 04 47	00 15 15	00 16 03	00 05 34				
	-51 31 45	-46.85	-52 00 56	-50 51 20	-51 01 33	-52 11 25				
1H0011-239	2.90	53.30	1.68	3.97	4.11	1.81	.640	.0049		A14?
	-23.93	-80.89	-24.30	-23.30	-23.55	-24.55		.0009		
	00 11 35	352.57	00 06 43	00 15 53	00 16 25	00 07 14				
	-23 55 46	-22.99	-24 17 52	-23 18 12	-23 33 06	-24 32 53				
1H0014-668	3.74	308.23	1.79	5.09	5.59	2.31	.532	.0019		
	-66.81	-50.24	-67.47	-65.96	-66.12	-67.65		.0004		
	00 14 58	318.95	00 07 09	00 20 20	00 22 22	00 09 13				
	-66 48 35	-58.60	-67 28 26	-65 57 21	-66 07 22	-67 39 06				
1H0014+111	3.73	109.77	2.73	4.58	4.72	2.87	.682	.0062		III Zw 2
	11.17	-50.55	10.93	11.73	11.41	10.61		.0015		
	00 14 54	7.88	00 10 55	00 18 19	00 18 53	00 11 28				
	11 10 15	8.76	10 55 44	11 43 30	11 24 34	10 36 52				
1H0016-257	4.16	43.70	2.92	5.24	5.40	3.07	.718	.0045		A15
	-25.79	-82.59	-26.18	-25.12	-25.39	-26.45		.0009		
	00 16 38	352.82	00 11 39	00 20 58	00 21 35	00 12 15				
	-25 47 30	-25.16	-26 10 43	-25 07 21	-25 23 40	-26 27 11				
1H0017+073	4.37	109.48	3.39	5.24	5.34	3.49	.512	.0034		
	7.36	-54.41	7.08	7.88	7.64	6.85		.0007		
	00 17 28	6.93	00 13 33	00 20 57	00 21 22	00 13 58				
	07 21 52	5.02	07 04 57	07 52 45	07 38 39	06 50 52				
1H0018+280	4.54	114.78	3.43	5.47	5.65	3.61	.740	.0041		A21
	28.05	-34.06	27.78	28.64	28.31	27.44		.0013		
	00 18 08	15.93	00 13 42	00 21 53	00 22 36	00 14 26				
	28 02 49	23.80	27 46 32	28 38 38	28 18 33	27 26 37				